NUMERICAL SIMULATION OF L-PBF ADDITIVE MANUFACTURING OF MEDIUM-MANGANESE STEEL FOR AUTOMOTIVE CRASH APPLICATIONS

K. ABBURI VENKATA[*], B. SCHOB[**], M. KASPROWICZ[***]

**Simufact Engineering part of Hexagon, 21079 Hamburg, Germany*
***Technische Universität Chemnitz, 09107 Chemnitz, Germany*
**** Wadim Plast Sp. z o. o., 05–816 Reguły, Poland*

DOI 10.3217/978-3-85125-968-1-19

ABSTRACT

Advanced High Strength Steels (AHSS) such as dual-phase steels are favoured for conventional crash box applications due to the excellent combination of strength and ductility. Generation three AHSS steels such as medium-Manganese Transformation Induced Plasticity (TRIP) steels are a possible alternative to fabricate prototype crash-boxes with equivalent properties of a conventional crash-box due to the TRIP effects. Laser Power Bed Fusion (L-PBF) can produce prototype crash boxes without the requirement of costly dies as in conventional manufacturing. This allows significant benefit in lead times and cost efficiency in manufacturing prototype crash boxes. A reliable numerical simulation tool can predict the L-PBF build process accurately while considering the thermo-metallurgical and mechanical behaviour of the material under multiple thermal cycles and aid the prototype design phase. In the current paper, an improved methodology for the simulation of L-PBF build process using finite element (FE) framework is presented. The proposed methodology provides better spatial resolution of the build process and considers the effects of phase transformation in the medium-Manganese TRIP steel during multiple thermal cycles thereby increasing the accuracy of numerical predictions. The model is set-up and analysed using commercial software Simufact Welding 2022 based on FE solver Marc 2021.2. A comparison of the simulation results with that of experimental analysis on a simple cantilever and a representative double-hat profile crash geometry indicates a very good agreement proving the suitability of the current approach for accurate simulation of L-PBF process whilst maintaining reasonable computational efficiency.

Keywords: L-PBF, additive Manufacturing, medium-Manganese TRIP steel, crash box, numerical simulation

INTRODUCTION

Deep-drawn parts are normally used in crash applications for body-in-white (BIW) vehicle structures [1, 2]. Automotive crash box is one of the most important parts for crash energy absorption and is equipped at the front end of a car [3]. The crash boxes connect the bumper cross member to the longitudinal beam and converts the dynamic

energy to deformation energy in case of frontal crashes. Manufacturing of these parts in conventional ways, even in prototyping phase, requires expensive tooling such as forming dies making the whole process time consuming and costly and therefore forms a serious bottleneck in the vehicle development process.

The need for improved fuel economy and reduced CO_2 emissions in automotive industry has led to significant developments in lightweight materials with higher strength [4]. The conventional materials such as low carbon steels and cast steels are replaced with Advanced High Strength Steels (AHSS) such as dual steels, TRansformation-Induced Plasticity (TRIP) steels due to their superior stiffness, strength, crash energy absorption capacity and low production costs in large quantities [5, 6]. In addition, the better formability of AHSS steels provides greater flexibility to optimise the component geometry.

Even with the flexibility in design and advanced materials, there are still significant lead times and costs incurred in conventional deep-drawing approaches owing to the expensive tooling and dies. Any design modification even in prototyping phase requires new tooling which can quickly escalate the costs and manufacturing lead times in the development process. On the other hand, Additive Manufacturing (AM) specifically, Selective Laser Melting (SLM) or Laser-Powder Bed Fusion (L-PBF) offer enormous design freedom while lowering the manufacturing times significantly [4].

The suitability of the L-PBF process to crash applications requires not only printing of the parts but also achieving the desired stiffness and crash performance of components produced by the AM process. The materials currently available for AM were not specifically developed for automotive industry which is further true for crash applications. Furthermore, the quality of materials produced by L-PBF process usually is unsuitable for crash applications. Therefore, appropriate post-processing is required to achieve the desired equivalent crash behaviour to that of conventional crash bodies.

With these considerations, a novel medium manganese TRIP steel is considered that was specifically developed for automotive applications using L-PBF process with minor modifications in the composition [7, 8]. In order to understand the overall influence of manufacturing history on the final crash performance of the component, a simulation model of the whole manufacturing process chain is indispensable.

In the present paper a simulation framework is presented for the numerical analysis of L-PBF process and post-processing of the novel medium manganese TRIP steel developed for crash applications. The simulation approach incorporates the multi-cycle Solid-State Phase Transformation (SSPT) experienced by this material during the build as well as the phase reversion during post-build heat treatment (HT). The results are validated with experimental investigations on a simple cantilever and a representative crash geometry (double hat profile) for the entire process chain.

EXPERIMENTAL INVESTIGATION

For the purpose of this research an experimental medium manganese steel was investigated, whose chemical composition is provided in Table 1. The details of the development of the steel and the material properties are already published elsewhere [8].

Table 1 Chemical composition of the experimental medium manganese steel

Element	Fe	Mn	Si	Al	P	C	S	O	N	H
(%)	balance	7.5–8.5	0.4–0.5	1.7–2.0	0–0.05	0.08–0.15	0–0.05	0–0.05	0–0.03	0–0.005

Two specimen geometries were fabricated to validate the simulation framework developed for the whole process chain. The first geometry is a simple cantilever specimen and the second is a complex representative geometry of the crash box namely double hat profile. The two specimens are shown in Fig. 1. The specimen dimensions are *72mm x 12mm x 15mm* and *118mm x 79mm x 200mm* for the cantilever and double hat geometries respectively. The nominal thickness of the double hat profile is 2 mm.

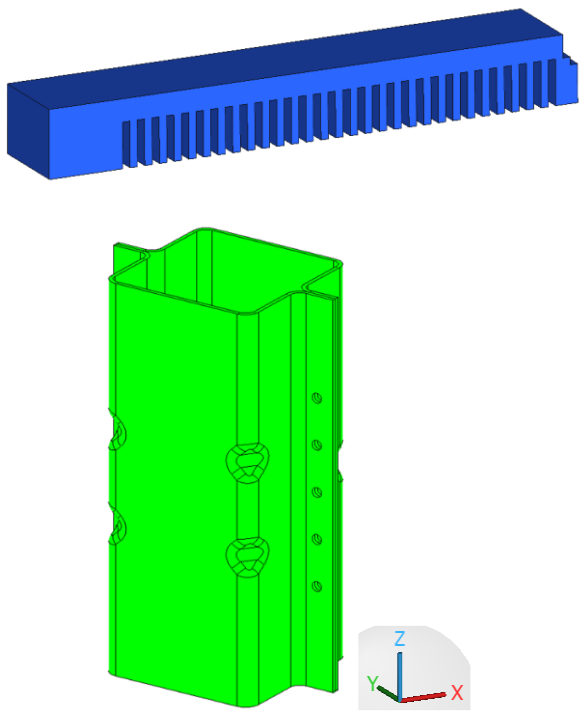

Fig. 1 Cantilever specimen (top) and double hat geometry (bottom)

The process parameters and heat treatment conditions for both geometries are provided in Table 2 and Table 3 respectively. The deflection of the cantilever geometry was measured in as built and HT conditions as +0.69mm and -0.25mm respectively, by using

a cutting plane at a height of 2.6mm from the base of the cantilever. Three-dimensional (3D) surface scan was performed on the double hat profile in build and HT conditions which were then used to validate the predictions from the simulations.

Table 2 SLM process parameters for double-hat geometry

Geometry	Laser power (W)	Laser speed (m/s)	Hatch distance (mm)	Layer thickness (mm)	Laser spot diameter (mm)
Cantilever	250	1.0	0.08	0.03	0.1
Double hat	265	1.0	0.09	0.03	0.1

Table 3 HT parameters for cantilever and double hat geometry

Geometry	Hold Temperature (C)	Hold time (h)
Cantilever	670	1.0
Double hat	670	6.0

Post-build global HT (heat treatment) is applied to the cantilever and double-hat geometry such that the content of austenite is significantly increased and the yield strength of the material is reduced to acceptable levels (~ 650 - 675 MPa) as that of conventional crash-box material. Careful investigation was undertaken to determine the right HT hold temperature and hold time such that the material has desired crash properties subsequently. It was determined that HT at 670 °C for 6 h on the double hat geometry resulted in best material properties with an austenite content of ~ 40% through experimental investigation. On the cantilever specimen, HT at 670 °C was applied for 1 h to achieve similar levels of austenite in the component after HT.

NUMERICAL INVESTIGATION

L-PBF BUILD

To ensure better accuracy of the L-PBF process and capture the transient thermal behaviour effectively, without entirely sacrificing computational efficiency, a different scheme of layer deposition than conventional approach is utilised. The details of the implementation and the approach were published in Ref. [8]. Based on the equivalent heat flux method, the power required for heating the entire track is calculated, keeping the heating time and the velocity of the robot the same as in the actual L-PBF process. To increase the accuracy of the predictions in the baseplate, a mesh refinement is used in the baseplate closer to the double-hat and the regions away from the part are meshed with coarser elements. First order hexahedral elements with an approximate size of 1 mm are used for meshing both the geometries. In order to facilitate the creation of structured mesh, the holes in the geometry are ignored as these can be later created via a machining simulation.

The model is set-up in commercial welding software Simufact Welding 2022 (based on Finite Element (FE) solver Marc 2021.2) using the dedicated DED (Directed Energy Deposition) module. Considering that the thermal behaviour of the molten material is the major contributor to the subsequent stress/strain and phase generation in L-PBF process, which is similar to that of DED fundamentally, the analysis was modelled using DED

module for ease of modelling and usage of certain in-built features. The mesh of the cantilever and double hat geometry along with the baseplates are shown in Fig. 2 and Fig. 3 respectively. The baseplate is considered as the same material as that of components and maintained at a temperature of 125 °C during the build process. To avoid rigid body movement, some nodes on the bottom surface of the baseplate are fixed. Temperature dependent thermal, mechanical properties and stress/strain curves generated using JMatPro were employed for the thermo-mechanical simulation of the SLM process. Element activation and deactivation is used to mimic the deposition of powder layers sequentially.

Furthermore, in L-PBF process, the build part is surrounded by powder that acts as a heat insulation and therefore, the heat loss to the surroundings is significantly different than that of a DED process. The simulation has been modified to take this into account by allowing only the top surface of the current layer to contribute to the heat losses. Since the available top surface for heat loss changes dynamically with every new track, this surface is recalculated after every subsequent new track is laid. In order to achieve this constant time stepping scheme was used for the heating process to recalculate the available surface for convection/radiation during L-PBF build.

The heat loss from the top surface is calculated using a convective heat transfer coefficient of 250 W/m2K and a radiation emissivity of 0.9. The contact heat transfer coefficient between the part and the baseplate is also modelled using a contact heat transfer coefficient of 1000 W/m2K. The entire cantilever and double-hat profile are considered as single parts with no contact considerations between one layer to another and therefore no contact heat transfer is modelled between individual layers of the specimens.

MULTI-CYCLE SSPT

During the build process the previously deposited layers will be subjected to multiple thermal cycles, leading to multiple phase transformation or even partial phase transformation during heating from martensite to austenite. Similarly, during cooling down, there can be several cases where the handling of retained austenite requires different approaches. To support the simulation of phase transformation of the material during multiple cycles and accurately predict the phases and the volume change effects, a new methodology is suggested where partial transformation during heating and handling of retained austenite for various cool down scenarios are proposed.

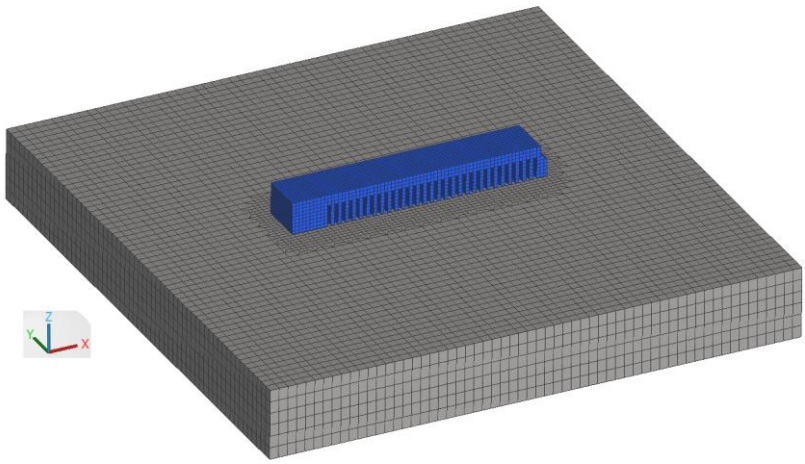

Fig. 2 FE mesh of the cantilever specimen with baseplate highlighting mesh refinement on baseplate

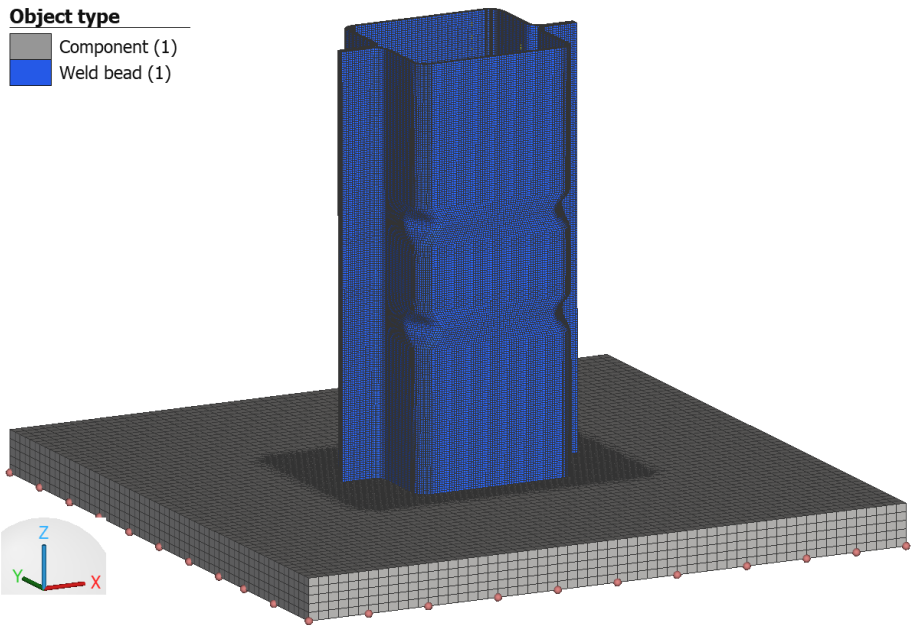

Fig. 3 FE mesh of the double hat geometry with baseplate highlighting mesh refinement on baseplate

This also handles the volume change effects during transformation. The phase change during heating is based on linear austenitisation rule and the martensite formation during cooling uses Koistinen-Marburger (KM) relation [9].

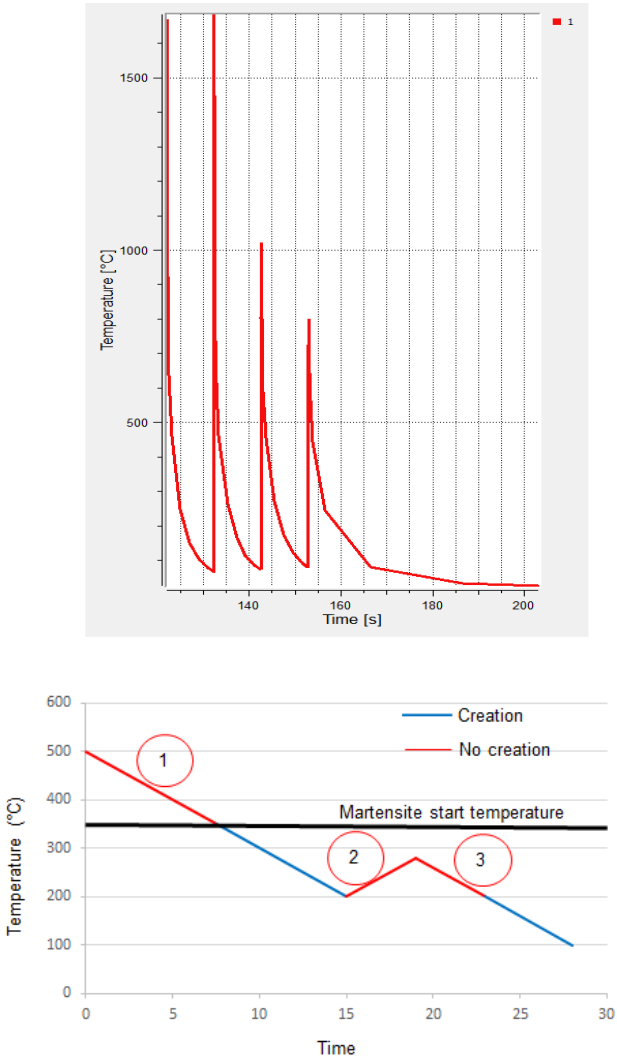

Fig. 4 Predicted multi-cycle thermal history (top) and phase evolution (bottom) during L-PBF build of medium manganese experimental TRIP steel

A schematic of the various cases for creation and non-creation of martensite during cool down is presented in Fig. 4 (bottom). The figure depicts only the cool down cases and the logic of martensite phase formation during multiple thermal cycles. The region shown as 1 indicates the cooling down of material but above martensite start temperature, whereas regions 2 and 3 indicate situations where the temperature of the material point during subsequent thermal cycles, does not go beyond martensite start temperature but is definitely more than the temperature state from previous cycle's cooling stage. In these situations, there will not be any martensite creation. The regions marked blue are those where martensite calculation is undertaken. In order to transform retained austenite to martensite, without reheating above AC1 (no fresh austenite), additional thermal or

mechanical energy should be available than the previous cooling state. This is due to increased stability of retained austenite due to increased amount of carbon, which also reduces the Ms (martensite start temperature) significantly. So further transformation is only achieved by cooling down below the previous cooling temperature. Since region 3 is above this, it is considered that the thermal energy available here is not enough to convert the retained austenite to martensite. Any TRIP effects present during the build process are ignored due to lack of any appropriate material data or evidence for such an effect during the build process.

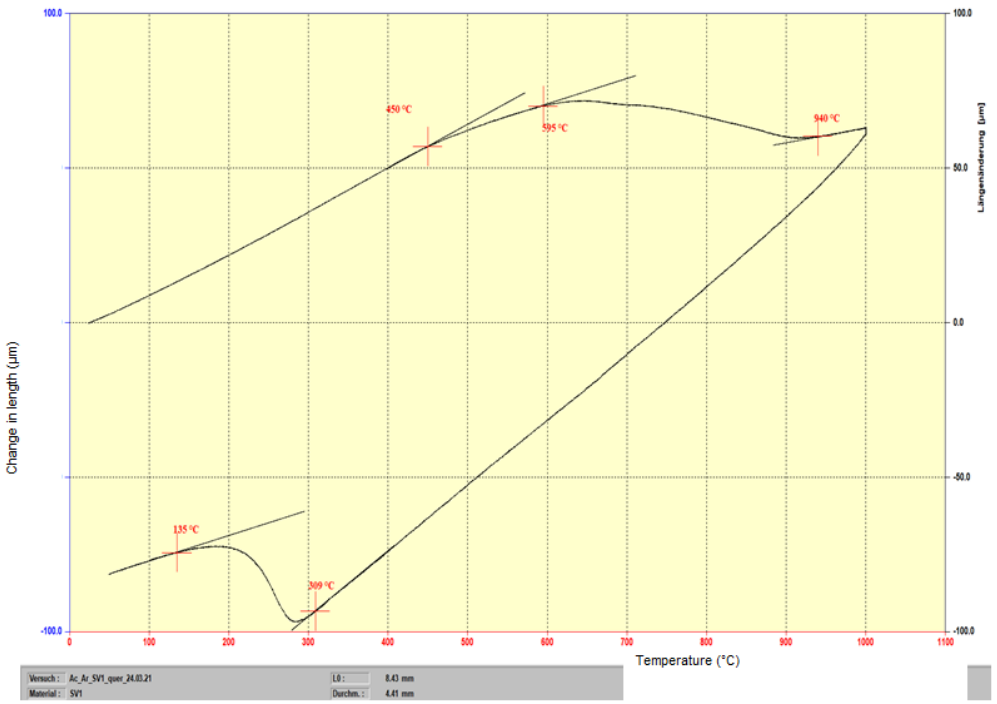

Fig. 5. Experimental dilatometry data for the proposed TRIP steel

The volume change associated with martensitic transformation has a significant influence on the stress/strain behaviour during welding process and this has been accounted using KM equation and the dilatational change measured through experiments as shown in Fig. 5. The tests were conducted with a heating rate of 30 K/s and a cooling rate of 100 K/s. Using the same dilatometry data, the temperatures AC1 (austenite start temperature), AC3 (austenite finish temperature), M_f (matensite finish temperature) and M_s (martensite start temperature) were identified. Linear austenitisation rule was applied between AC1 and AC3 to calculate the percentage of austenite formation as a function of temperature.

HT SIMULATION AND BASEPLATE REMOVAL

Post-build HT was simulated using the HT module in Simufact Welding 2022 as part of process-chain modelling, in order to achieve the require microstructure and material properties for crash applications. During HT, history from build process was considered as initial state and the residual stresses/strains, local hardening and phase distribution were predicted for the cantilever and double hat geometries. This allowed for the relaxation and redistribution of residual stresses/strains from the build process during HT due to reduced yield strength at higher temperatures. In addition, the martensite and austenite phases were also predicted using KM equation, after HT, resulting in further modification of the material properties. The KM parameters were calibrated such that the martensite and reverted austenite phase fractions were ~60% and 40% respectively after HT. Creep was not considered during HT simulation due to lack of appropriate material data.

After HT, the baseplate was removed through machining which was also simulated as part of process-chain modelling. The resulting residual stresses/strains from the HT simulation were provided as initial state to the cutting simulation which was also modelled using Simufact Welding 2022. Since there was no thermal behaviour during cutting, elastic-plastic material behaviour was assumed during the cutting process. The baseplate was removed using "DEACTIVATE" elements option which simulated the removal of material and relaxation of internal stresses/strains due to the deformation of the part. The phase behaviour was also not considered as the material phases are not expected to alter during the cutting operation.

MAPPING OF RESULTS FOR CRASH SIMULATION

The purpose of the process-chain simulation and analyses was so that the actual material state prior to crash simulation, arising from the manufacturing history, is accurately captured. Consequently, the aim of the research is to analyse the material state through predictions throughout the process-chain and finally apply this as initial state to the crash simulations. The build, HT and subsequent baseplate removal simulations were all analysed using 3D hexahedral elements whereas crash simulation requires a shell mesh. So, it was essential to map results such as stresses and local hardening after baseplate removal simulation, to a shell mesh. This was achieved using a third-party mapping software MpCCI mapper developed by Fraunhofer SCAI [10]. The kinematic result quantities such as residual stresses/strains were mapped from the hexahedral mesh to the shell mesh. This was achieved through aligning the positions of both meshes in a coordinate system.

RESULTS AND DISCUSSION

BUILD PROCESS

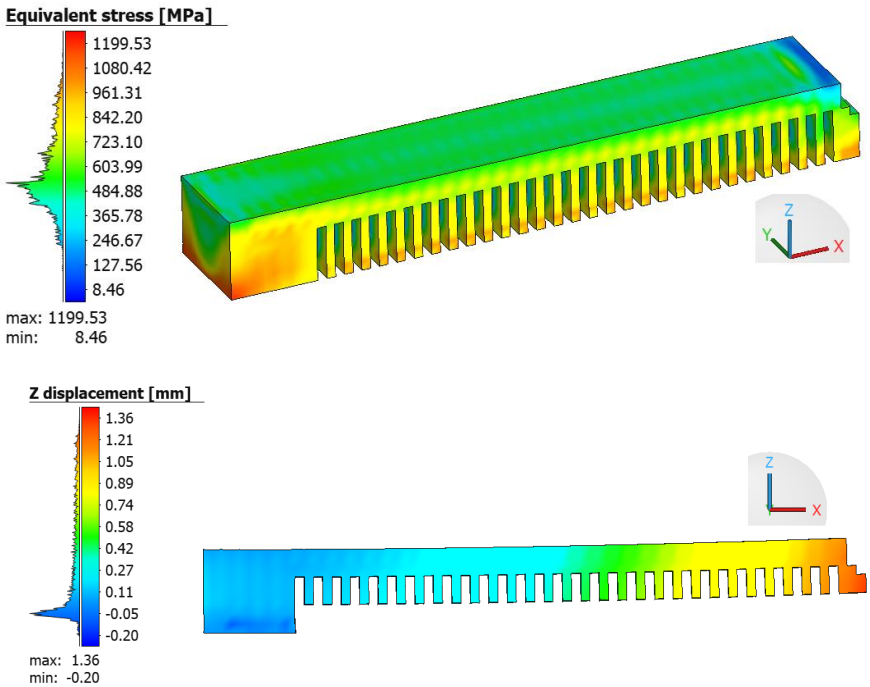

Fig. 6 Predicted equivalent stress in cantilever geometry after build (top) and displacement of the cantilever after cutting in build state

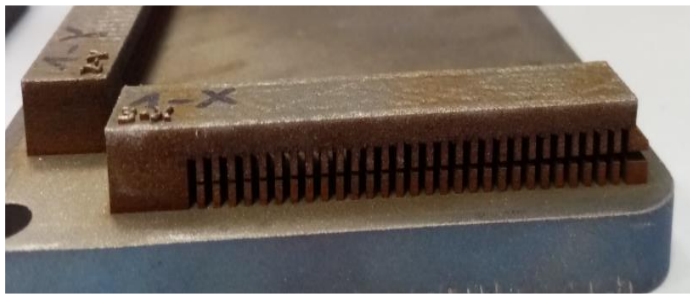

Fig. 7 Printed cantilever for experimental investigation and validation of simulation

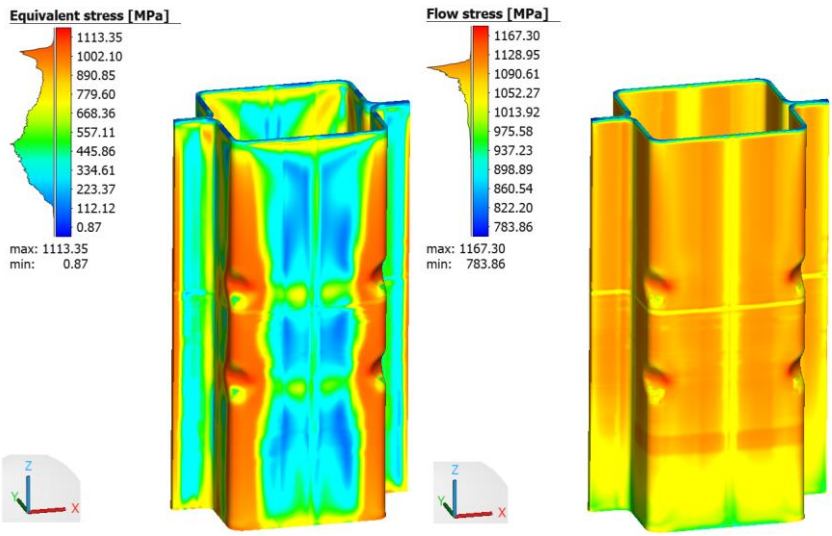

Fig. 8 Predicted equivalent stress (left) and flow stress in the double-hat specimen (right)

Based on the simulation methodology presented in above sections in addition to the material phase transformation modelling, the thermal history in the double-hat profile is predicted which was used to predict the phase evolution, stresses and deformation in the part. Fig. 6 shows the equivalent stress distribution predicted in the cantilever (top) and the deflection of the cantilever after cutting from the baseplate is shown below. It is to be noted that in both cases the cantilever is attached fully and partially to the baseplate respectively, although it is not displayed. The positive deflection of the cantilever is +1.36 mm which is larger than the measured deflection (see EXPERIMENTAL INVESTIGATION). However, this discrepancy can be attributed to the presence of another cantilever built on the same baseplate as evident from Fig. 7, which can alter the thermal behaviour during the build process. Nevertheless, the deflection direction matches between the predictions and measurements.

Fig. 8 shows the equivalent stress distribution predicted in the double hat specimen on the left side and the flow stress/hardening on the right. Results indicate that AM process introduces considerable residual stresses and hardening in the part due to repetitive thermal cycles. The distribution of martensite phase and total deformation is presented in Fig. 9. It can be seen from the phase distribution that the martensite phase is not the same across various regions in the layer. The same is observed in the temperature predictions in the part as depicted in Fig. 10 (left) where the temperature predictions are different between layers and also within a certain layer. The analysis has been terminated when the temperature at every integration point reached below 50 °C to save computational time.

The image on the right side in Fig. 10 shows the track-based deposition of the layer profile from left to right. It is interesting to note that the temperature in the previously deposited layer is different across various tracks in the same layer, owing to the differences in the deposition and cooling times/sequence within the layer. This shows that with the proposed methodology greater resolution is achieved within a layer. These differences in the cooling times/sequence led to differences in the predicted martensite

fractions within a layer. Since the stresses are calculated as a weighted sum of the individual phase fractions, the hardening and the flow stress values are also different within a layer, thereby providing greater spatial resolution and improved accuracy in the overall performance of simulation.

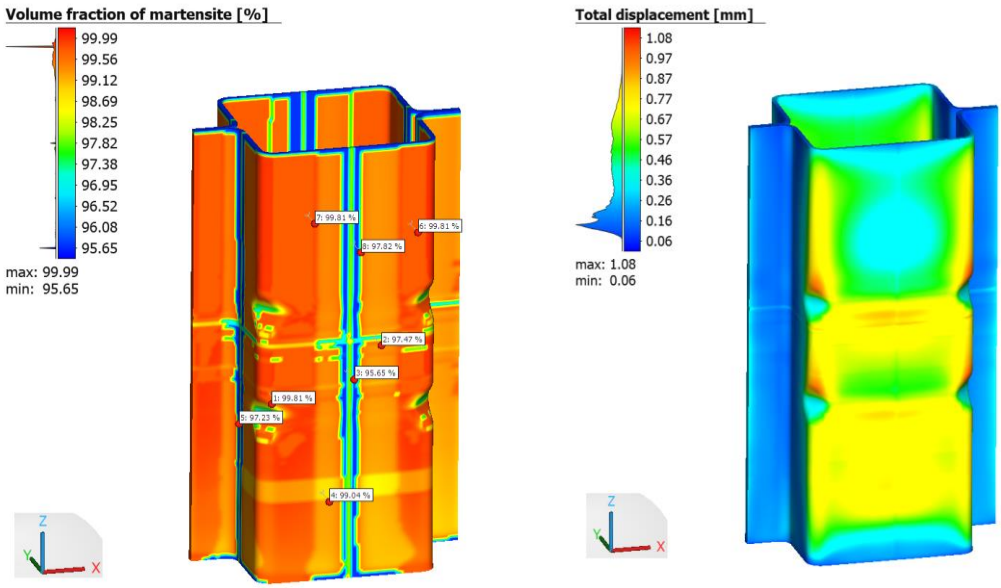

Fig. 9 Martensite volume fraction as a function of component dimensions (left) and total displacement (right) in the double-hat specimen due to L-PBF build

HT AND BASEPLATE REMOVAL

The residual stresses (top) and deformation (below) in the cantilever specimen subsequent to HT and partial cutting of the baseplate are shown in Fig. 11. It is interesting to note that the deformation profile indicates a downward deflection with a magnitude of -0.64 mm after HT. This agrees qualitatively well with experimental results where the deflection of the cantilever was negative after HT. Fig. 12 shows the predicted martensite phase in the cantilever specimen after HT process.

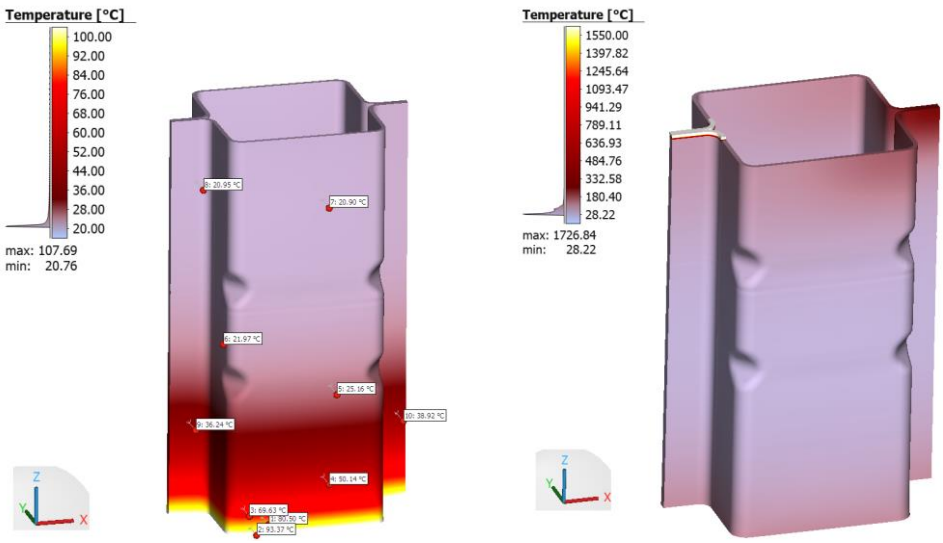

Fig. 10 Predicted temperature distribution in the double-hat specimen (left); track based element activation (right)

The predicted martensite phase (left) and total deformation (right) in the double hat specimen after global HT process are displayed in Fig. 13. It is seen that after HT, the overall martensite fraction drops to 60% as opposed to ~99% from the build simulation. Fig. 14 shows the equivalent stress in the specimen after HT (left) and removal of baseplate (right) respectively. It is visible that the residual stresses are reduced significantly due to HT compared to that of the build simulation, which are further relaxed with the removal of baseplate. This clearly demonstrates that the process-chain simulation has captured the real material behaviour satisfactorily.

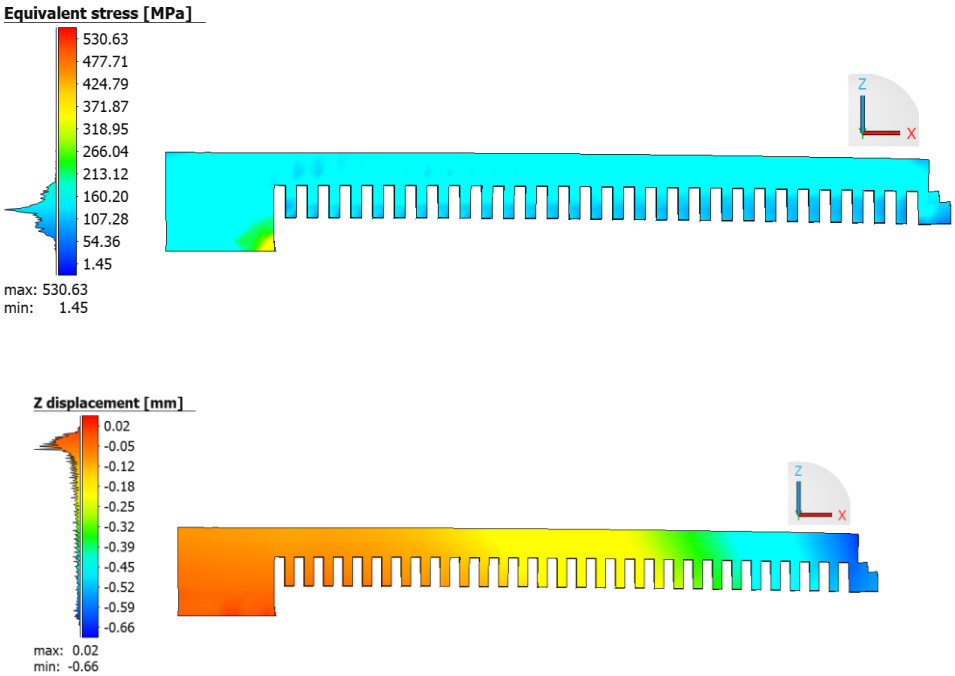

Fig. 11 Predicted residual stresses (top) and deflection (below) in the cantilever specimen after HT and removal of baseplate

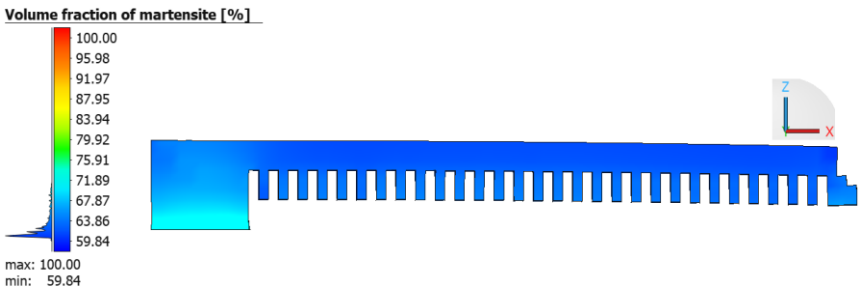

Fig. 12 Predicted martensite phase in the cantilever specimen after HT

VALIDATION OF SIMULATION PREDICTIONS

To validate the build simulation and the predicted behaviour of the cantilever and double hat profile, comparison of predictions with experimental measurements was performed. For the cantilever profile, the measured deflection of the cantilever in build and HT conditions, due to partial cutting of the baseplate was compared with that from predictions. A good agreement was observed in the deflection profiles qualitatively with measurements.

The experimentally measured 3D surface scan of the double hat specimen is compared against that of predicted profile/surface of the geometry after build simulation using GOM Inspect 2018 tool. The comparison of the scanned profile of the geometry with that of predicted scanned profile is displayed in Fig. 15. The measurements were made on the specimen with the baseplate still attached, after the build. It is observed that the predictions match closely with experiments especially closer to the baseplate. As the build height increases, there is a variation of ~ 1.2 mm between the measured and predicted profiles. This can be explained due to the discrepancies between the predicted and actual thermal profile inside the build chamber as the build height increases. Another reason to which this difference can be ascribed to is the assumed material properties in the simulation. Since these were extracted using JMatPro rather than actual material characterisation, this can lead to some variation in the results.

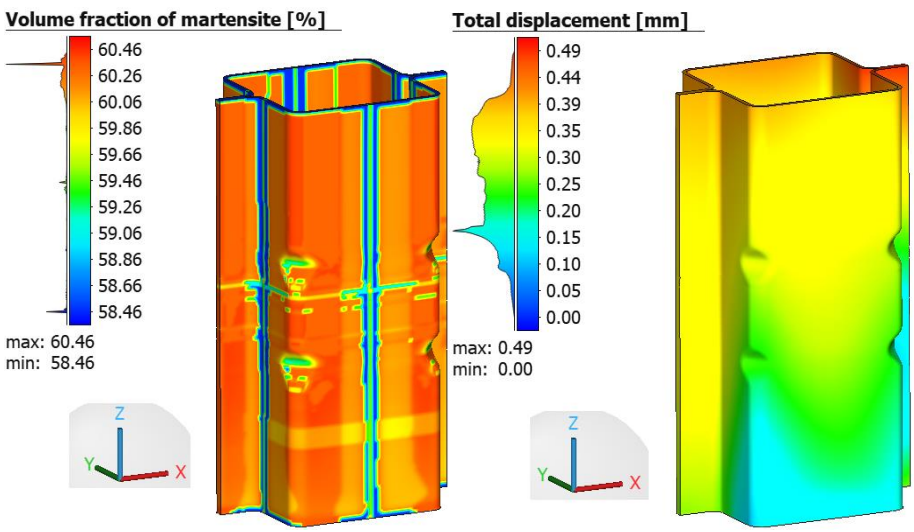

Fig. 13 Predicted martensite phase (left) and total deformation (right) in the double hat specimen after HT and removal of baseplate

The predicted stress relaxation due to HT and removal of baseplate of the double hat profile is also validated with experimental measurement as shown in Fig. 16. The measured surface of the double hat specimen after HT and removal of baseplate is compared against measured surface. It is observed that the simulation predictions match very well with those from experiments validating the process chain simulation.

MAPPING OF RESULTS

The mapped values of the stresses and strains onto the shell mesh are shown in Fig. 17 top and bottom respectively. Comparing Fig. 14 (right) and 17 (below), it can be agreed upon that the results from the hexahedral mesh were mapped accurately onto the shell mesh. This shell mesh with the mapped stresses and hardening will be used subsequently in

crash simulation. In this manner the entire manufacturing and process history of the crash specimen is considered in crash simulation for greater accuracy.

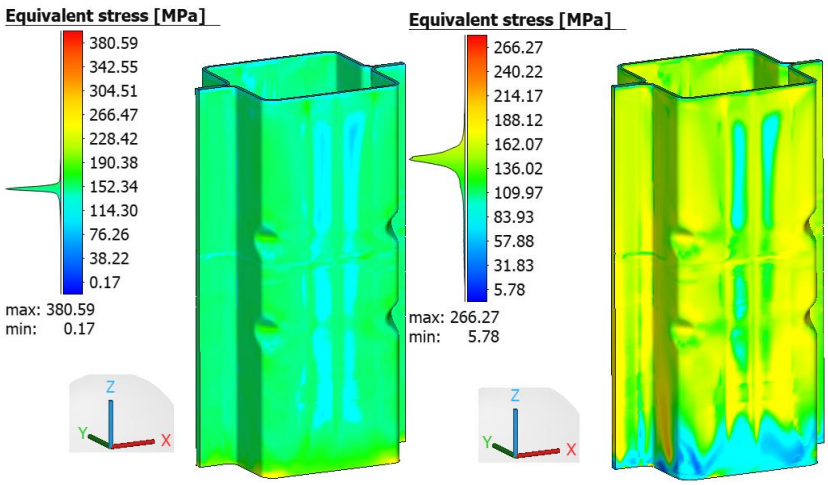

Fig. 14 Predicted residual stresses in the double hat specimen after HT (left) and removal of baseplate (right)

CONCLUSIONS

The paper presented a framework for the process-chain simulation for manufacturing prototype components for crash applications using L-PBF. The build process, HT and baseplate removal are simulated to predict the final material state for crash applications. Advanced material behaviour such as multi-cycle phase transformation and phase change during build and HT processes are captured in the simulation. The process-chain is tested on two different geometries namely cantilever and double hat profile to study the suitability of the simulation framework for L-PBF manufacturing of crash components. Based on the work presented the following conclusions can be drawn.

1. Simulation of L-PBF with increased spatial and temporal resolution increases the accuracy of the predictions.
2. It is essential to capture the multi-cycle phase transformation of the material during L-PBF build for accuracy and reliability in predictions.
3. Validation of the simulation framework on simple geometries such as cantilever can improve confidence in the predictions.
4. The simulation framework developed enables the consideration of manufacturing history and appropriate material state in a valid manner for high fidelity applications such as crash using L-PBF process.

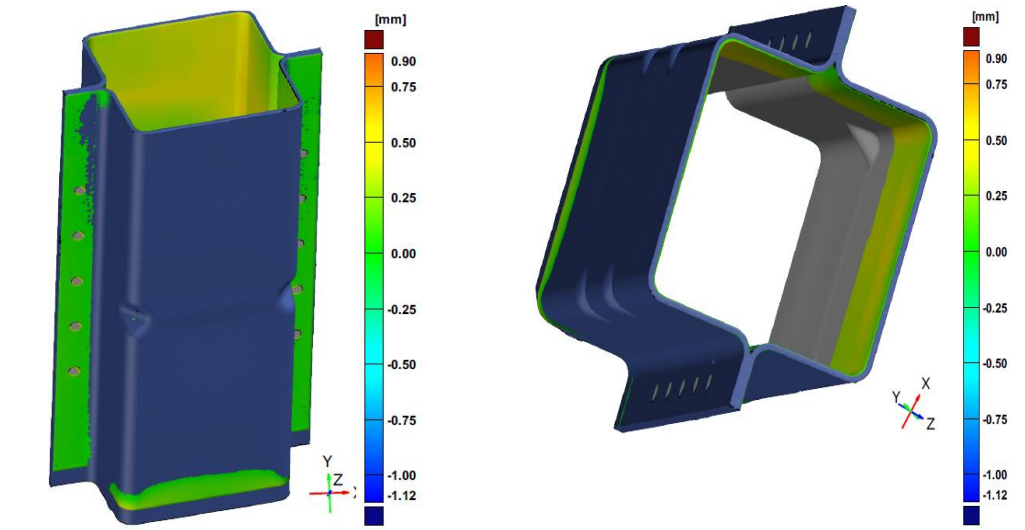

Fig. 15 Comparison of predicted and measured surface profile of double-hat geometry after build

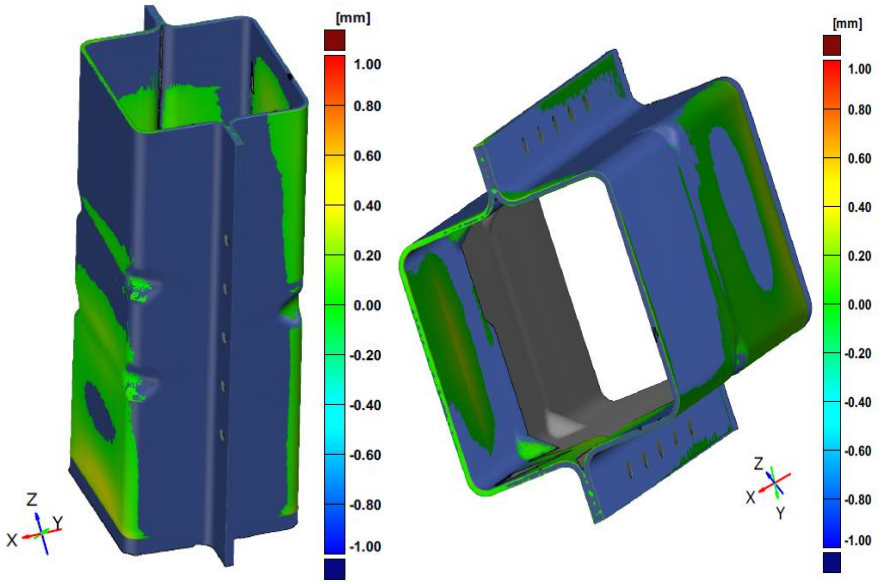

Fig. 16 Comparison of predicted and measured surface profile of double-hat geometry after HT and removal of baseplate

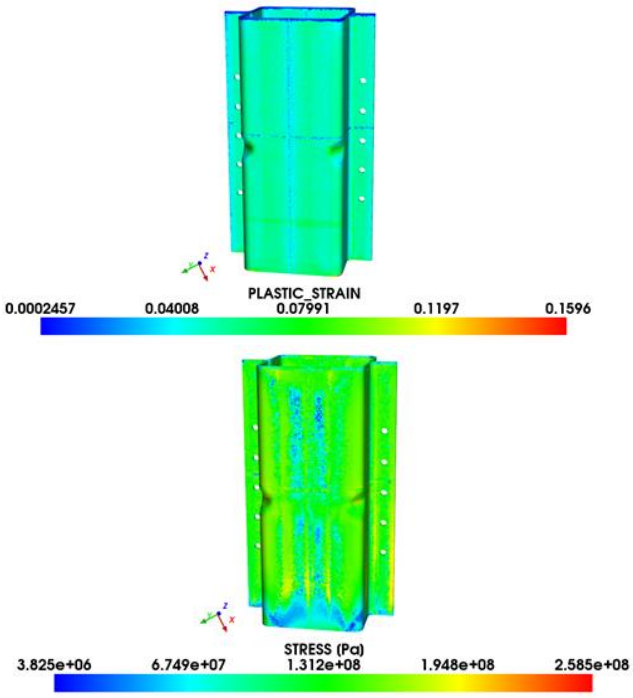

Fig. 17 Mapped equivalent plastic strain (top) and stress (below) on double hat shell mesh with holes

ACKNOWLEDGEMENTS

This work was performed within the project "Additive Manufacturing Technologies for Crash loaded structural Components (AM-Crash)" and supported by the Federal Ministry of Education and Research (BMBF) and by the Polish National Centre for Research and Development (NCBR) under international programme M-ERA.NET 2 Cofund Financial support is gratefully acknowledged. The authors are grateful for all the support, experimental and validation data from project partners.

References

[1] C.D. HORVATH: 'Advanced steels for lightweight automotive structures, Materials, Design and Manufacturing for Lightweight Vehicles', *Woodhead Publishing*, 2010, Pages 35-78, ISBN 9781845694630, https://doi.org/10.1533/9781845697822.1.35.

[2] A. DEB: 'Chapter 11 - Crashworthiness design issues for lightweight vehicles, Materials, Design and Manufacturing for Lightweight Vehicles' (Second Edition), *Woodhead Publishing*, 2021, Pages 433-470, ISBN 9780128187128, https://doi.org/10.1016/B978-0-12-818712-8.00011-2.

[3] N.S. YUSOF, S. SAPUAN, M.T.H. SULTAN, M. JAWAID, M. MALEQUE: 'Design and materials development of automotive crash box: a review', *Ciência & Tecnologia dos Materiais*, 29, 2017, 129-144. 10.1016/j.ctmat.2017.09.003.

[4] A. BORRELLI, G. D'ERRICO, C. BORRELLI, R. CITARELLA: 'Assessment of Crash Performance of an Automotive Component Made through Additive Manufacturing', *Applied Sciences*, 10(24), 9106, 2020, https://doi.org/10.3390/app10249106.

[5] J. GALAN, L. SAMEK, P. VERLEYSEN, K. VERBEKEN, Y. HOUBAERT: 'Advanced high strength steels for automotive industry', *Revista de Metalurgia*, 48(2), 18-131, 2012, doi: 10.3989/revmetalm.115.

[6] R. KUZIAK, R. KAWALLA, S. WAENGLER: 'Advanced high strength steels for automotive industry', *Archives of Civil and Mechanical Engineering*, 8(2), 2008, DOI: 10.1016/S1644-9665(12)601.

[7] M. HOEFEMANN et al.: 'Ein niedriglegierter Stahlwerkstoff für die Laseradditive Fertigung Prozesskette und Eigenschaften', In: Lachmayer R., Rettschlag K., Kaierle S. (eds) *Konstruktion für die Additive Fertigung 2019*, Springer Vieweg, Berlin, Heidelberg, 2020, https://doi.org/10.1007/978-3-662-61149-4_3.

[8] K. ABBURI VENKATA et al.: 'Accurate numerical prediction of thermo-mechanical behaviour and phase fractions in SLM components of advanced high strength steels for automotive applications', *Technologies for Lightweight Structures* 5(1), 2021, pp. 41-50, Special issue: 5th International MERGE Technologies Conference (IMTC), 1st-2nd December 2021, Chemnitz.

[9] D. KOISTINEN, R. MARBURGER: 'A General Equation Prescribing the Extent of the Austenite-Martensite Transformation in Pure Iron-Carbon Alloys and Plain Carbon Steels', *Acta Metallurgica*, 7, 59-60, 1959, https://doi.org/10.1016/0001-6160(59)90170-1.

[10] https://www.scai.fraunhofer.de/en/cross-sectional-topics/software-and-services-for-the-automobile-industry/mpcci-mapper-in-practice.html.